24th INTERNATIONAL CONGRESS ON SOUND AND VIBRATION
23–27 July 2017, London

MODELLING THE DEAGGLOMERATION OF NANOPARTICLE INCLUSIONS BY ULTRASONIC MELT PROCESSING

Anton Manoylov, Georgi Djambazov and Koulis Pericleous

University of Greenwich, Computational Science and Engineering Group, Greenwich, London, UK
email: G.Djambazov@greenwich.ac.uk

Bruno Lebon

Brunel University London, Brunel Centre for Advanced Solidification Technology, Uxbridge, UK

The aerospace and automotive industries are seeking advanced materials with low weight-to-strength ratio, such as light alloy-based metal matrix composites (MMC) with nanoparticle reinforcements. However, van der Waals and adhesive forces between nanoparticles result in large agglomerates that compromise the final properties of MMCs. Ultrasonic melt processing is a potential technology for de-agglomerating these clusters and producing samples with improved properties via grain refinement. This paper considers two hypotheses of cluster de-agglomeration: the breakup of a cluster due to the growth of gas contained in the cluster and the stripping of nanoparticles by pulsating neighbouring bubbles.
Keywords: acoustic cavitation, particle de-agglomeration, light alloy melts

1. Introduction

Aluminium-based metal matrix composites offer a high strength-to-weight ratio and are of great interest to the aerospace and automotive industries. However, introducting nanoparticles into the melt is not without difficulty [1]: nanoparticles are not wetted by the molten metal and interaction forces between them are dominant in the nanoscale [2]. Nanoparticles tend to form large, strong clusters that require large stresses to be dispersed.

Ultrasonic melt processing is a potential technology for agglomerate dispersion. Furthermore, ultrasonic treatment improves significantly the functional quality and thermo-physical properties of light alloy melts in other ways [3, 4]. Beneficial effects include the degassing of dissolved gases (usually hydrogen), improvement in the wetting and activation of inclusions, enhanced nucleation, and refinement of the grain structure [5].

The study of particle de-agglomeration aims to identify the forces responsible for the formation of particle clusters and the conditions enabling these forces to be overcome. In this paper, the dispersion of nano-particles in an aluminium crucible is studied by coupling a high-order acoustic model [6] to a model of particle clusters based on the Discrete Element Method (DEM) [7, 8].

2. Theory

2.1 Governing Equations

2.1.1 *Wave Equation*

Sound propagation in a pure liquid is modelled by the continuity and momentum equations:

$$\frac{\partial p}{\partial t} + v_j \frac{\partial p}{\partial x_j} + \rho c^2 \frac{\partial v_j}{\partial x_j} = S \tag{1}$$

$$\frac{\partial v_i}{\partial t} + v_j \frac{\partial v_i}{\partial x_j} + \frac{1}{\rho}\frac{\partial p}{\partial x_i} = 0 \tag{2}$$

where p is the acoustic pressure, v_i are the velocity components, ρ is the liquid density, and c is the speed of sound in the liquid. The source S contains the bubbles' contributions to acoustic pressure.

2.1.2 *Bubble Dynamics*

Bubbles are assumed to remain spherical as they oscillate radially in a pressure wave. The effect of bubble shape distortions on their resonant frequency is of the order of 2 % [9] and the surface tension between aluminium and hydrogen (the common gas phase in aluminium melts) is large. These two effects justify the assumption of sphericity for cavitating bubbles in ultrasonic melt processing. The Rayleigh-Plesset equation [10] can then be used to represent the bubble dynamics:

$$R\ddot{R} + \frac{3}{2}\dot{R}^2 = \frac{p_s}{\rho} \tag{3}$$

with

$$p_s = p_b + p_v - \frac{2\sigma}{R} - \frac{4\mu\dot{R}}{R} - p_0 - p_\infty - p \tag{4}$$

R is the bubble radius, p_0 is the atmospheric pressure, p_b is the pressure inside the bubble, p_v is the liquid vapour pressure, p_∞ is the pressure from the ultrasonic source, σ is the surface tension between the liquid and the bubble gas, and μ is the dynamic viscosity of the liquid.

The bubble pressure p_b is given by

$$p_b = p_{g,0}(R_0/R)^{\mathbf{3\kappa}} \tag{5}$$

where $p_{g,0}$ is the initial bubble pressure and κ is the polytropic exponent.

2.2 Discretization Method

2.2.1 *Acoustic Cavitation Modelling*

Sound propagation and bubble dynamics are solved using the procedure described in [6]. Equations (1) and (2) are solved using a high-order staggered finite difference method. Spatial derivatives are evaluated on a 6-point stencil, with mirroring of variables at solid boundaries. The pressure above the liquid free surface is fixed to 0 Pa, to model a 180° phase shift upon reflection. A 4-point stencil is used to evaluate temporal derivatives [11]. The Rayleigh-Plesset equation (3) is solved explicitly using the 4th order Merson's method, with multi-staging for solver stability [12].

2.3 Particle Modelling

The DEM modelling considers particles in a Lagrangian framework. Particles are assumed to be spherical. The linear and angular momentum equations are derived for each particle based on the fluid-particle, particle-particle interaction forces and torques as well as body forces:

$$m_i \frac{\partial^2 \bar{x}_i}{\partial t^2} = \overline{F^b} + \overline{F^f} + \sum_{j\neq i} \overline{F_{ij}^p}, \tag{6}$$

$$J_i \frac{\partial^2 \bar{\phi}_i}{\partial t^2} = +\overline{T^f} + \sum_{j\neq i} \overline{T_{ij}^p} \tag{7}$$

where index i corresponds to i-th particle, m and J are the particle's mass and moment of inertia, x – position, φ – orientation, F – forces, T – torques, and upper indices b, f and p correspond to body, fluid-interaction and particle-interaction forces. The overbar denotes a vector. As particles are spherical, the angular momentum equation is used to evaluate angular velocity instead of orientation.

2.3.1 *Particle-particle forces*

Typically, the spring-dashpot model accounts for particle-particle interaction [13, 14] during collisions, in which e.g. [15] friction and adhesion forces are also added. The adhesion can be defined as van der Waals attraction forces acting on elastically deformed surfaces. It is considered to be the

driving force behind the formation of particle clusters. The model [7, 8] used in this study (Fig. 1) is based on that of [15].

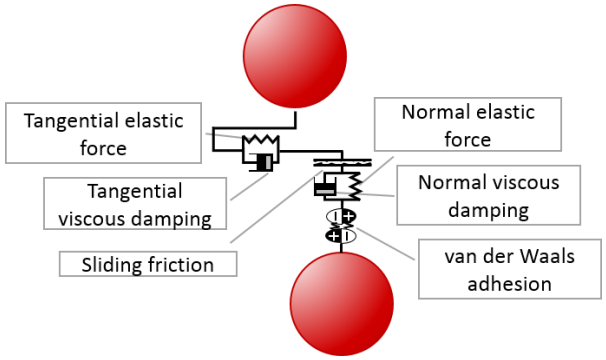

Figure 1 Schematic illustration of particle-particle interaction forces

Other forces acting on particles come from particle-fluid interactions. These forces are listed in Table 1. Discussion on other fluid-particle interaction forces and their models can be found in [13, 16, 17]. R_p denotes particle radius – not to be confused with average bubble radius R in (3).

Table 1 Particle-fluid interaction forces

Force	Model	Comments
Drag force (di Felice model)	$F_d = \frac{1}{2}\rho_f (v-u)^2 C_d \pi R_p^2 \varepsilon^{-\beta}$ $Re_p = \frac{\rho_f}{\mu_f}\alpha_f R_p \lvert v-u \rvert$ $C_d = \left(0.63 + \frac{4.8}{\sqrt{Re_p}}\right)^2$ $\beta = 3.7 - 0.65 e^{-0.5(1.5 - log_{10} Re_p)^2}$	R_p – particle radius Re_p – particle Reynolds number C_d – drag coefficient β – empirical coefficient ε – void volume fraction u, v velocities of particle and fluid ρ_f – fluid density
Gravity/buoyancy	$F_g = (1 - \rho_f/\rho_p)mg$	ρ_p – particle material density
Pressure gradient force	$F_p = \frac{\rho_f}{\rho_p} m \left(\frac{du}{dt} - [(v-u)\cdot\nabla]u\right)$	
Saffman lift force	$F_s = -2.18 \frac{\rho_f}{\rho_p} m \frac{(v-u)\times\omega}{\sqrt{Re_p \lvert\omega\rvert R_p \lvert v-u\rvert}}$	ω – angular velocity of the particle
Magnus lift force	$F_m = -\frac{3}{4}\frac{\rho_f}{\rho_p} m \left(\frac{1}{2}\omega - \Omega\right) \times (v-u)$	Ω – vorticity of the fluid flow
Magnus torque	$M_m = 8\pi\mu R_p^3 \left(\frac{1}{2}\omega - \Omega\right)$	

2.3.2 *Coupling*

A one-way coupling between the acoustic solver and particles model was developed, with the effect of particles on the fluid flow and cavitation being neglected. To implement the particle-fluid interaction forces, fluid flow variables (pressure and velocity) and cavitation variables (average bubble radius R, bubble concentration θ, bubble interface pressure P_b and bubble interface velocity *dR/dt*) are passed to the particles model. These variables are averaged over their respective computational cells and within a time step of the acoustic solver.

3. Problem Description

3.1 Material Properties

Table 2: Material properties for aluminium at 700 °C [3, 18, 19].

Material Property	Aluminium
Sound speed (c m s^{-1})	4600
Density (ρ kg m^{-3})	2375
Dynamic viscosity (μ mPa s)	1.0

Surface tension (σ N m^{-1})	0.860
Vapour pressure (p_v Pa)	0
Bulk modulus (K GPa)	41.2
Ratio of specific heats (γ)	1.4

Table 2 lists the material properties used in the numerical experiments. The gas phase (hydrogen) is assumed to be adiabatic, i.e. $\kappa = \gamma = 1.4$. Table 3 lists the particle properties. Interfacial energy values are required for evaluating the adhesion force. This differs from the surface tension at the gas/fluid interface. The interfacial energy values of 0.2 and 2.0 J/m^2 used in this study are hypothetical and do not correspond to a particular solid-liquid interface. Real values of interfacial energy depend on many factors, such as wetting, presence of gaseous phase, conductivity of the fluid, and particle material as well as particle material microstructure. More details about evaluating the interfacial energy can be found in [7, 20].

Table 3 Particle properties

Particle property	**Value**	**Units**
Diameter	10	µm
Young's modulus	450	GPa
Poisson's ratio	0.185	-
Density	2600	kg/m^3
Friction coefficient	0.3	-
Interfacial energy	0.2, 2.0	J/m^2

3.2 Geometry

3.2.1 *Ultrasonic treatment*

Figure 2a represents a typical experimental setup for the ultrasonic treatment of aluminium [21] and corresponds to the simulation described in [6]. The crucible walls are reflective to sound waves, whilst a 180° phase shift occurs at the free surface. The liquid height is 17.5 cm and the diameter of the cylindrical base is 12 cm. This crucible volume corresponds to 5.2 kg of aluminium at 700 °C. The operating frequency of the transducer is 17.7 kHz. The sonotrode tip is immersed 2 cm below the free surface.

3.2.2 *Particles positioning*

In this study, clusters were formed of 55 densely packed particles as shown in Figure 3a. Clusters were positioned in 6 rows of 1 cm gap and 9 columns of 0.5 cm gap as shown in Figure 2b. The first row is 1 cm below the sonotrode. The y-position of the first row is -3 cm from the top of the crucible. The particle spatial configuration is 3-dimensional and de-agglomeration is also modelled in 3D space. The acoustic solution represents a cross-section of an axially symmetric process.

3.3 De-agglomeration

The de-agglomeration of particles involves breaking up large particle clusters into smaller ones or into individual particles. De-agglomeration was observed as a result of the ultrasonic processing of aluminium [1, 5, 22, 23]. During ultra-sonication of aluminium, hydrogen bubbles form, oscillate and collapse, creating chaotic and intensive velocity pulses. The beneficial effect of ultrasound on de-agglomeration is attributed to these pulses. Little is known about the exact timing, location and amplitude of these pulses. In [22], the pulse velocity is estimated to be up to 3 km/s. The cavitation events are shown to be highly localised, i.e. the energy of the pulse dissipates quickly with both time and distance. In this study, the bubble surface velocity, *dR/dt*, obtained from the acoustic solver is used as a measure of the magnitude of such pulses. As the quantities related to the cavitation solver are averaged across computational cell and time step, they are attributed to the behaviour of a representative bubble originating in the computational cell. It is assumed that velocity pulses propagate spherically originating from the initial cluster positions. The magnitude of the pulse is taken as *dR/dt*

value within the 5R distance from the origin and then it decays as inverse squared distance, so as to maintain the fluid flow rate constant. The example of breaking a cluster of 55 particles by a spherical pulse is shown in Figure 3b. More detailed study of de-agglomeration of particles caused by spherical velocity pulses (no coupling to the acoustic solver) is provided in [7].

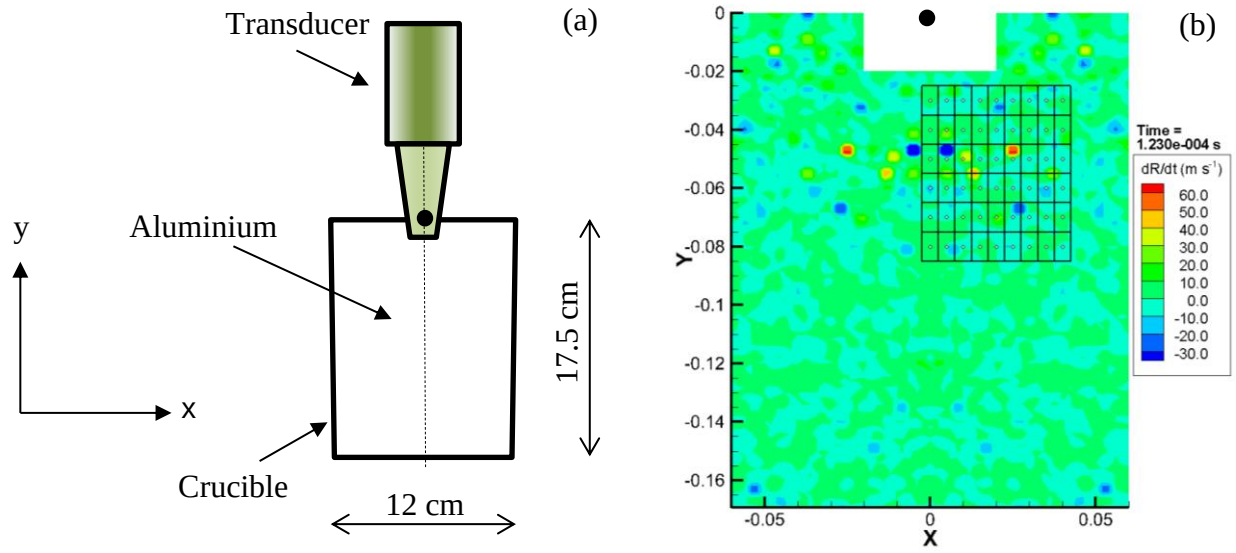

Figure 2: (a) Schematic of aluminium treatment setup [21]. The origin of the domain marked as a black dot is at the intersection of the axis and the plane 2cm above the vibrating surface of the sonotrode; (b) contour plot of dR/dt values and initial positioning of 54 particle clusters.

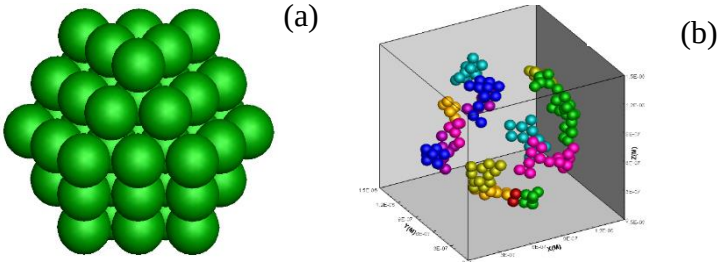

Figure 3 (a) Cluster consisting of 55 densely packed particles; (b) example of cluster breakup caused by a spherical pulse originating in the centre of the cluster; pulse velocity magnitude 100 m/s. Colours indicate sub-clusters formed as a result of breaking. Red particles are isolated (single-particle clusters).

The de-agglomeration of a particle cluster is quantified as the average distance from particles that initially belonged to the cluster to their geometrical centre, scaled by the particle radius:

$$D_{agg} = \frac{1}{R_p N_p} \sum_i \left| \bar{x}_i - \frac{1}{N_p} \sum_j \bar{x}_j \right| \quad (8)$$

where N_p (=55) is the number of particles in a cluster, R_p is a particle radius (constant in this study), x_i denotes position and bar is for the vector notation. Particles of 5 μm radius and interfacial energies of 0.2 and 2.0 J/m^2 were subjected to the spherical velocity pulses caused by cavitation.

4. Results

4.1.1 *Acoustic Cavitation*

Figure 4 shows the pressure profile and bubble distribution along a plane across the axis of the crucible. The bubble cloud is denser below the sonotrode, as is expected: due to acoustic shielding, the ultrasonic energy is attenuated by the cloud under the sonotrode, hence prohibiting the formation

of further bubble structures away from the sonotrode. This is also consistent with experimental evidence of large pressure decay away from the radiating source [22]. Bubbles survive at anti-nodes along the sonotrode axis (represented by grey spheres).

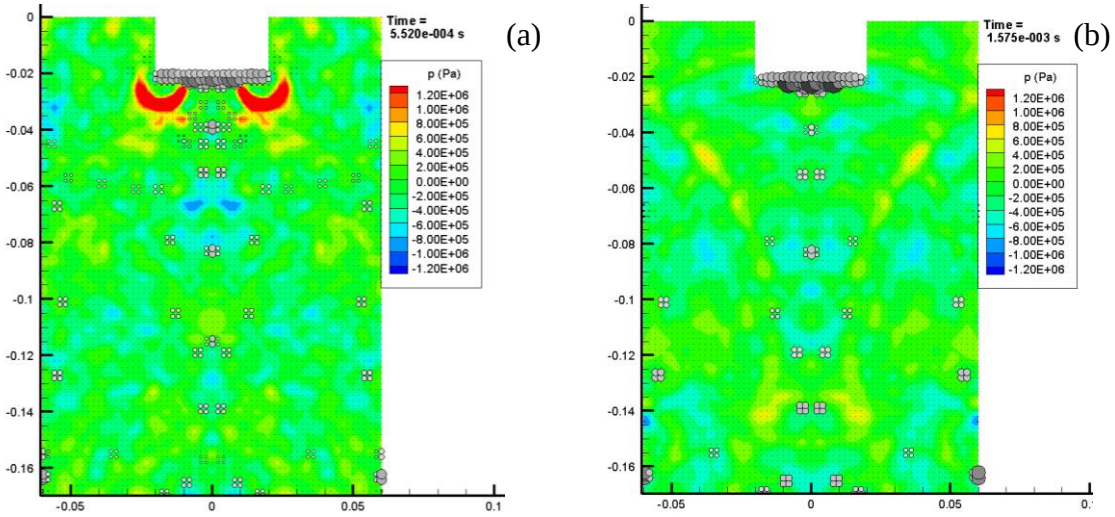

Figure 4: Pressure contour and bubble distribution in crucible at (a) t = 552 μs and (b) t = 1575 μs.

4.1.2 *De-agglomeration of particles*

Figure 5a illustrates the magnitude of the pulse *dR/dt* at the initial position of 23rd cluster (x=2cm, y=-5cm). Series of *dR/dt* values are marked on Figure 5a as peaks $p_1,..,p_7$ preceded by valleys $v_1,..v_2$. Values corresponding to these peaks and valleys are listed in Table 4. The non-dimensional de-agglomeration values D_{agg} corresponding to the cluster of particles with interfacial energies γ=0.2 and 2.0 J/m^2 respectively, are shown in Figure 5b. Table 5 provides images of particles at peaks $p_1,..,p_7$. The colouring is the same as in Figure 3b. Note that the peaks p_1 and p_2 are unable to cause visible damage to the cluster with either interfacial energy. Peak p_3 despite having a lower value (1.42 m/s) than peak p_1 (2.2 m/s) is able to break the lower energy cluster. This can also be confirmed by the D_{agg} plot in Figure 5b. The valley-peak difference is however higher for p_3-v_3 than for p_1-v_1 which allows us to conclude that peak-valley fluctuation of *dR/dt* is a factor responsible for de-agglomeration. The cluster with higher energy (Table 5 lower row) does not break until p_8 where the peak–valley difference is 18 m/s. A significant rise in D_{agg} for the higher energy cluster can be observed between p_7 and v_8 which corresponds to the bubble implosion rather than growth. Increase of the D_{agg} value can be explained by movement of the cluster away from the origin of the pulse, so that the more remote part of the cluster is subjected to the implosion by a lesser degree than the other part. When the implosion originates inside a cluster where particles are in tight contact, the elastic rebound of the particles can cause the cluster to de-agglomerate. On the other hand, in the absence of particle contact, the implosion causes a decrease in D_{agg} as seen in Fig. 5b on the lower energy cluster curve between p_7 and v_8.

5. Conclusions

The coupling of an acoustic solver with a DEM model for particles was implemented, providing an efficient numerical tool for studying the mechanisms of particle clusters breakup due to cavitation. The fluctuations of interfacial bubble velocities obtained from the acoustic solver were correlated to the breakup of clusters, as illustrated in Table 5 and quantified by a non-dimensional parameter D_{agg} defined in (8). Both higher and lower interfacial energy clusters eventually broke up which suggests that even averaged values of *dR/dt* are sufficiently large for the breakup to occur. Further analysis of

the behaviour of clusters placed in 54 positions below the sonotrode allows the determination the regimes of sonication that are favourable to the de-agglomeration of particles.

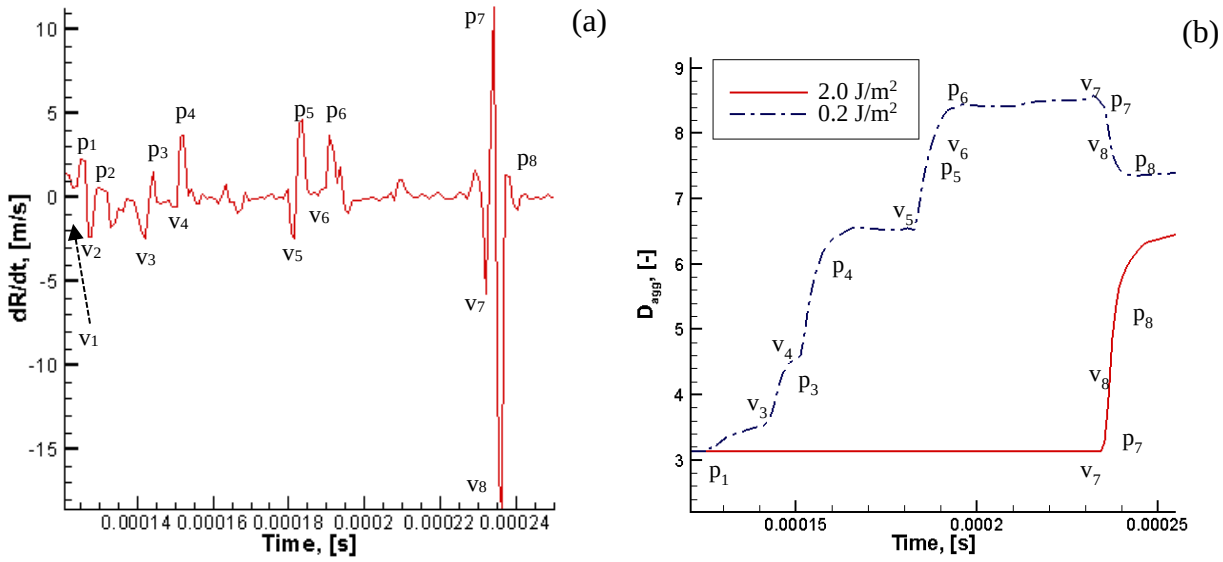

Figure 5 (a) the value of *dR/dt* at the initial position of 23rd cluster (x=2cm, y=-5cm), time range until 0.12-0.25ms of processing; (b) Non-dimensional de-agglomeration parameter D_{agg} as defined by (8).

Table 4 Values of dR/dt corresponding to the valleys and peaks marked on Figure 5b

Valley	Time [ms]	dR/dt [m/s]	Peak	Time [ms]	dR/dt [m/s]	p-v [m/s]
v_1	0.123	0.57	p_1	0.125	2.2	1.53
v_2	0.127	-2.32	p_2	0.128	0.53	2.85
v_3	0.142	-2.29	p_3	0.144	1.42	3.71
v_4	0.149	-0.5	p_4	0.152	3.68	4.18
v_5	0.181	-2.13	p_5	0.183	4.52	6.65
v_6	0.188	1.71	p_6	0.190	3.60	1.89
v_7	0.232	-5.57	p_7	0.234	10.96	16.53
v_8	0.235	-17.4	p_8	0.237	1.33	18.73

Table 5 Spatial configuration of particle at peaks p_1..p_7; top row - γ=0.2 J/m^2; bottom row - γ=2.0 J/m^2

p_1	p_2	p_3	p_4	p_5	p_6	p_7	p_8
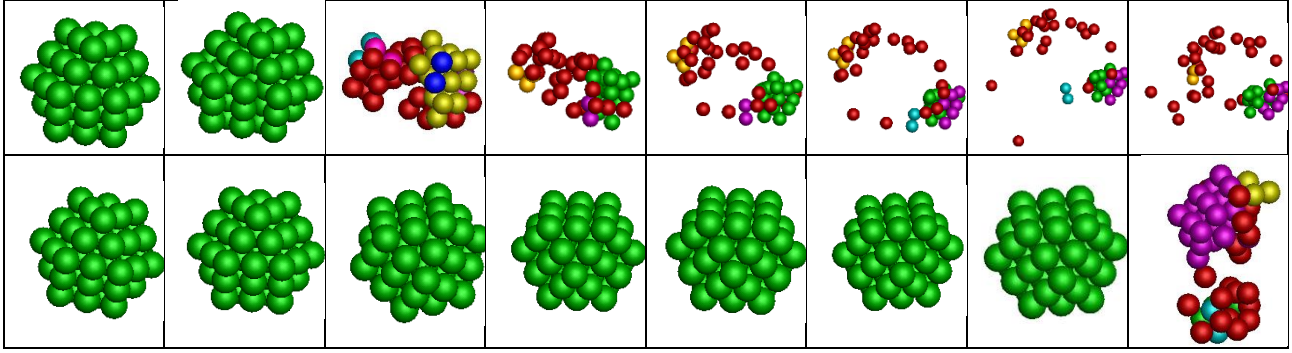							

REFERENCES

1. Kudryashova, O. B., Vorozhtsov, S. A., Khrustalyov, A. and Stepkina, M. Ultrasonic Dispersion of Agglomerated Particles in Metal Melt, *AIP Conference Proceedings*, **1772**, 020013, (2016).

2. Sauter, C., Emin, M. A., Schuchmann, H. P. and Tavman, S. Influence of Hydrostatic Pressure and Sound Amplitude on the Ultrasound Induced Dispersion and De-Agglomeration of Nanoparticles, *Ultrason Sonochem,* **15** (4), 517-523, (2008).
3. Eskin, G. I. and Eskin, D. G., *Ultrasonic Treatment of Light Alloy Melts*, CRC Press, Boca Raton, FL, USA (2014).
4. Campbell, J. Effects of Vibration During Solidification, *International Metals Reviews,* **26** (1), 71–108, (1981).
5. Eskin, G. I., Makarov, G. S. and Pimenov, Y. P. Effect of Ultrasonic Processing of Molten Metal on Structure Formation and Improvement of Properties of High-Strength Al-Zn-Mg-Cu-Zr Alloys, *Advanced Performance Materials,* **2** (1), 43–50, (1995).
6. Lebon, G. S. B., Tzanakis, I., Djambazov, G., Pericleous, K. and Eskin, D. G. Numerical Modelling of Ultrasonic Waves in a Bubbly Newtonian Liquid Using a High-Order Acoustic Cavitation Model, *Ultrasonics Sonochemistry,* **37**, 660-668, (2017).
7. Manoylov, A., Bojarevics, V. and Pericleous, K. (2015) Modeling the break-up of nano-particle clusters in aluminum- and magnesium-based metal matrix nano-composites, *Metallurgical and Materials Transactions A*, 46 (7). pp. 2893-2907, (2015)
8. Manoylov, A., Djambazov, G., Bojarevics, V. and Pericleous, K., Multiple timescale modelling of particle suspensions in metal melts subjected to external forces, In: *ECCOMAS Congress 2016 VII European Congress on Computational Methods,* (2016)
9. Strasberg, M. The Pulsation Frequency of Nonspherical Gas Bubbles in Liquids, *The Journal of the Acoustical Society of America,* **25** (3), 536, (1953)
10. Plesset, M. S. The Dynamics of Cavitation Bubbles, *J. Appl. Mech.,* **16**, 277–282, (1949).
11. Djambazov, G. S., Lai, C. H. and Pericleous, K. A. Staggered-Mesh Computation for Aerodynamic Sound, *AIAA Journal,* **38** (1), 16–21, (2000).
12. Laevsky, Y., *Intel® Ordinary Differential Equation Solver Library*, Intel Corporation, (2008).
13. Zhu, H.P., Zhou, Z.Y., Yang, R.Y., Yu, A.B. Discrete particle simulation of particulate systems: Theoretical developments. *Chemical Engineering Science* 62:3378 – 3396, (2007)
14. Goniva C., et al., A Multi-purpose Open Source CFD-DEM Approach 8th International Conference on CFD in Oil & Gas, Metallurgical and Process Industries, SINTEF/NTNU, Trondheim Norway, (2011)
15. Thornton, C., Yin, K. K. Impact of elastic spheres with and without adhesion. *Powder Technology* 65:153-166, (1991)
16. Marshall, J. S., Discrete-element modelling of particulate aerosol flows. *J. Comp. Physics* 228:1541-1561, (2009)
17. Marshall, J. S. and Li, S. *Adhesive Particle Flow: A Discrete-Element Approach*, Cambridge University Press, New York, (2014)
18. Speight, J. G. and others, *Lange's Handbook of Chemistry*, McGraw-Hill New York (2005).
19. Waller, I. and Ebbsjo, I. On the Calculation of the Bulk Modulus of a Liquid Metal Using the Pressure Fluctuations in a Microcanonical Ensemble and a Numerical Application to Liquid Aluminium, *Journal of Physics C: Solid State Physics,* **12** (18), L705, (1979).
20. Israelachvili, J. N., *Intermolecular and Surface Forces*, Academic Press, New York, (1985).
21. Tzanakis, I., Lebon, G. S. B., Eskin, D. G. and Pericleous, K. A. Characterisation of the Ultrasonic Acoustic Spectrum and Pressure Field in Aluminium Melt with an Advanced Cavitometer, Journal of Materials Processing Technology, 229, 582–586, (2016).
22. Y. Yang, J. Lan and X. Li, "Study on bulk aluminium MMNC fabricated by ultrasonic dispersion of nano-sized SiC particles in molten aluminum alloy" Materials Science and Engineering A, 380, 378–383, (2004)
23. X. Li. Y. Yang, D. Weiss, "Ultrasonic cavitation based dispersion of nanoparticles in aluminum melts for solidification processing of bulk aluminum matrix nano-composite: Theoretical study, fabrication and characterization", AFS Transactions, American Foundry Society, Schaumburg, IL, USA (2007)
24. Tzanakis, I., Lebon, G. S. B., Eskin, D. G. and Pericleous, K. Investigation of the Factors Influencing Cavitation Intensity During the Ultrasonic Treatment of Molten Aluminium, *Materials and Design,* **90**, 979–983, (2016).